Dynamic environment-induced multistability and critical transition in a metacommunity ecosystem

Ramesh Arumugam,[1,2] Sukanta Sarkar,[1] Tanmoy Banerjee,[3] Sudipta Sinha,[4] and Partha Sharathi Dutta[1]

[1]*Department of Mathematics, Indian Institute of Technology Ropar, Rupnagar 140 001, Punjab, India*

[2]*Department of Biology, McGill University, Montreal, Quebec, Canada H3A 1B1*

[3]*Chaos and Complex Systems Research Laboratory, Department of Physics, University of Burdwan, Burdwan 713 104, West Bengal, India*

[4]*Department of Chemistry, Indian Institute of Technology Ropar, Rupnagar 140 001, Punjab, India*

(Received 31 January 2019; published 20 March 2019)

We study a metacommunity model of consumer-resource populations coupled via dispersal under an environment-dependent framework, and we explore the occurrence of multistability and critical transition. By emphasizing two magnitudes acting on a dynamic environment at temporal and spatial scales, the coupled system with simple diffusive coupling and the nonlinear environmental coupling enables various interesting complex dynamics such as bistability, multistability, and critical transitions. Using the basin stability measure, we find the probability of attaining each alternative state in a multistable region. In addition, critical transitions (one from a high to a low species density and the other from a low to a high species density) are identified at different magnitudes in the presence of stochastic fluctuations. We also explore the robustness of critical slowing-down indicators, e.g., lag-1 autocorrelation and variance, to forewarn the critical transition in the metacommunity model. Further, a network structure also identifies synchronization and multiclustering for a different choice of initial conditions. In contrast with the earlier studies on dynamic environmental coupling, our results based on the defined magnitudes provide important insights into environmental heterogeneity, which determines the set of environmental conditions to predict metacommunity stability and persistence.

DOI: 10.1103/PhysRevE.99.032216

I. INTRODUCTION

Systems of coupled oscillators construct an efficient framework to study interacting oscillatory processes relevant to different fields such as physics, chemistry, biology, ecology, engineering, and many other disciplines of science and technology [1,2]. The impact of such studies becomes more advantageous due to the fact that natural systems are rarely isolated and hence their dynamics can be explored using potential models of interacting oscillators. Extensive research on network of coupled oscillators explored a diversity of cooperative phenomena, such as synchronization [3,4], phase-locking [5,6], oscillation quenching [7], and chimera states [8–10].

In the context of coupled oscillators, coupling plays a crucial role in determining their dynamics [11]. In natural systems, units interact with each other directly through diffusion and also indirectly, e.g., via a common environment. Particularly, this type of coupling is very much relevant in ecology where species interact with common resources as well as shared resources [12]. However, existing studies with generic oscillators considered the shared resource as a linear one [11], which deviates from reality. In the context of ecology diffusion (or dispersion) is generally considered as a linear process, however, other forms of coupling are typically nonlinear. For example, the interaction between resources and consumers can be nonlinear in nature, e.g., via the type-II functional response [13]. Functional response determines how consumption rate varies with resource density. The type-II functional response is a saturating nonlinear function such that the consumption rate increases up to a level and then saturates with increasing resource density.

In complex spatial ecosystems, habitats where species reside are highly dynamic in nature [14]. Furthermore, multiple tropic interactions [15,16] and its distribution with underlying spatial heterogeneity [17,18], and the magnitude of environmental conditions affect the metacommunity dynamics [19]. Investigations on numerous coupled nonlinear systems and stochastic oscillators describe the theoretical understanding of various biological mechanisms arising in metacommunity ecosystems [20,21]. Particularly, different types of network topologies emphasize the structure of habitat connectivity, dispersal, and spatial distributions on ecosystem functioning [10,22,23]. Therefore, to model and study spatial ecosystems by incorporating proper forms of coupling that encapsulates local as well as shared interactions are challenging tasks.

In this paper, we take into account two types of species interaction in the coupling, namely diffusive coupling and *nonlinear* environmental coupling, to incorporate various complexities of metacommunity systems [24]. In fact, these couplings characterize the consumer-resource interactions in three fundamental ways: (i) the interaction within the patch (interaction with a local resource), (ii) the interaction between the patches (species migration), and (iii) the interaction through a common dynamic environment (interaction with a shared resource). Due to the spatial pattern of landscape structure, the magnitude of species interactions acting on the dynamic environment over time has a profound impact on the species persistence. Here, we aim to address the following questions: How do the magnitudes of spatially distributed

populations acting on a dynamic environment affect the metacommunity dynamics? What is the range of the magnitudes (fractions) at temporal and spatial scales that can promote metacommunity stability and persistence?

Here, we explore both deterministic as well as corresponding stochastic metacommunity models using two magnitudes defined on the dynamic environmental coupling. The considered magnitudes determine various complex dynamics of the coupled system, such as bistability, multistability, and critical transition. In particular, the existing bistability and multistability consist of contrasting dynamical states in a combination of both the equilibrium and nonequilibrium states. Subsequently, using the concept of basin stability [25], we find the probability of attaining a particular state in a multistable region if initial conditions are chosen randomly. This determines whether the metacommunity will persist or face extinction via a *critical transition* [26,27]. In the vicinity of a tipping point, when a system suddenly (in a relatively short span of time) shifts from one stable state to another under the influence of small stochastic perturbations, it is known as a critical transition. We find that although critical transitions occur here in proximity to a saddle node bifurcation, still the critical slowing-down indicators such as lag-1 autocorrelation and variance do not always successfully forewarn of an upcoming transition. We also study the system dynamics if the deterministic coupled system incorporates the environmental stochasticity as well as a network structure with a large number of interacting habitats.

The paper is organized as follows: First, the metacommunity model with simple diffusive and nonlinear environmental coupling is defined in Sec. II. Further, two different magnitudes are defined in Sec. III based on the species interactions with the considered coupling. The existence of multistability and critical transitions using both deterministic and stochastic cases is explained in Secs. III A and III B, respectively. Similar qualitative dynamics in a network structure consisting of more patches (nodes) is explored in Sec. III C. In Sec. IV, the conclusions and the ecological relevance of multistability, multiclustering, and critical transitions are discussed in detail.

II. MATHEMATICAL MODEL

We investigate a spatially structured Rosenzweig-MacArthur (RM) model as a metacommunity system under an environment-dependent framework [19]. In particular, this model characterizes the consumer-resource interactions in fragmented habitats of an ecosystem and also species migration in a dynamic environment. Here each habitat (patch) consists of a local resource density (V) and a consumer density (H). We consider two types of coupling: (i) habitats are connected through the migration of consumer species via diffusion, and (ii) a dynamic environment with a shared resource density (E) governed by a logistic growth function, which is accessible to all the consumers from different interacting habitats [12,24]. In this case, in contrast to the diffusion process, the coupling function is considered to obey the type-II functional response. The metacommunity model under an environment-dependent framework is formulated as

$$\frac{dV_i}{dt} = rV_i\left(1-\frac{V_i}{K}\right) - \frac{\alpha_i V_i}{V_i+B}H_i, \tag{1a}$$

$$\frac{dH_i}{dt} = H_i\left(\beta\frac{\alpha_i V_i}{V_i+B} - m\right) + \gamma\frac{\epsilon_i E}{E+C}H_i + d(H_{i+1}-2H_i+H_{i-1}), \tag{1b}$$

$$\frac{dE}{dt} = r_1 E\left(1-\frac{E}{K_1}\right) - \sum_{i=1}^{n}\frac{\epsilon_i E}{E+C}H_i, \tag{1c}$$

where the patch index is denoted by $i = 1, 2, \ldots, n$. It is important to note that the dynamics of the consumer (H_i) in the ith patch depends on both the local resource (V_i) as well as the shared environmental resource (E). In Eq. (1a), the logistic growth function in each patch consists of r and K denoting the growth rate and the carrying capacity of the local resource (V_i), respectively. In type-II functional response, α_i and B denote the predation (consumption) rate and the half-saturation constant of the consumers, respectively. Also, the conversion efficiency through predation and the natural mortality rate of the consumer are denoted by β and m, respectively. Moreover, in the logistic growth function of the shared resource (E), r_1 and K_1 denote the growth rate and the carrying capacity, respectively. ϵ_i denotes the predation rate of the consumer with respect to E. In other words, ϵ_i denotes the strength of environmental coupling that connects each ith patch to the common dynamic environment. Also, γ and C represent the consumer's conversion efficiency and the half-saturation constant over the environmental resource. Each patch is connected to the nearest-neighbor patches through migration of the consumer species with dispersal strength (d), in other words local coupling strength. Overall, the local coupling strength (d) connects only interacting patches, whereas the environmental coupling strength (ϵ_i) connects each ith patch to the common dynamic environment (E).

III. RESULTS

Initially, we consider a metacommunity model that consists of two patches under an environment-dependent framework. The schematic representation of the consumer interactions over the local resource and the shared environmental resource are described in Fig. 1. As we aim to address how the magnitude of consumer interactions alters the metacommunity dynamics, specifically stability and persistence, we define *two different magnitudes (or fractions)* of consumer interactions in terms of local and shared resources: (i) the magnitude of *environmental predation over local predation* ($F_{\epsilon\alpha}$), and (ii) the magnitude of *consumer interactions over a shared resource* ($F_{\epsilon_1\epsilon_2}$) (to be elaborated on later in this section). In the following subsections, we discuss key results governed by these two factors. Numerical simulations including a bifurcation analysis of the deterministic system have been carried out using the continuation package XPPAUT [28]. The stochastic simulations have been performed in MATLAB (R2015b).

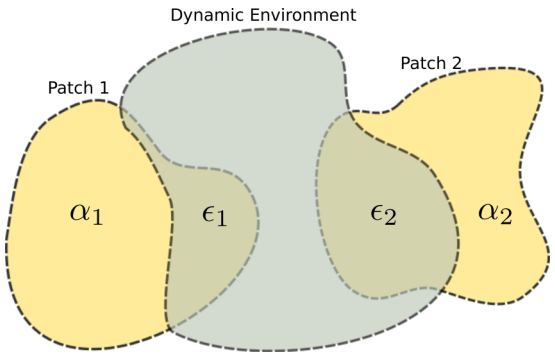

FIG. 1. Schematic representation of the coupled system (1) with two patches in a dynamic environment. Here α_i denotes the consumption (predation) rate of the consumer species in the ith patch over its local resource V, whereas ϵ_i denotes the consumption over the environmental resource E.

A. Effects of variations in the magnitude of environmental predation over local predation ($F_{\epsilon\alpha}$)

In the metacommunity system (1) (with $n = 2$), first we define the magnitude of consumer (H) interactions as a fraction of environmental predation (ϵ) over the predation (α) in a local resource [12]:

$$F_{\epsilon\alpha} = \frac{\epsilon}{\alpha} = \frac{\text{Environmental predation rate}}{\text{Local predation rate}}.$$

For our present study, in both patch 1 and patch 2, the consumption rates on the local resource are set to be identical (i.e., $\alpha_1 = \alpha_2 = \alpha$). Also, the consumer species consumption rates on the shared environmental resource are set to be identical (i.e., $\epsilon_1 = \epsilon_2 = \epsilon$). The magnitude $F_{\epsilon\alpha}$ determines both the temporal and spatial configurations of the consumer populations (H) in the metacommunity.

1. Existence of multistability with variations in $F_{\epsilon\alpha}$

We explore the qualitative dynamics of the coupled system (1) at different magnitudes (fractions) of consumer (H) interactions on local (V) and shared (E) resources. The coupled system with both diffusive and environmental coupling exhibits collective dynamics such as synchronization and multistability at different $F_{\epsilon\alpha}$. In particular, the stable oscillations from all the interacting patches show perfectly synchronized behavior. Using a one-parameter bifurcation diagram for varying the fraction ($F_{\epsilon\alpha}$), the qualitative dynamics of resource

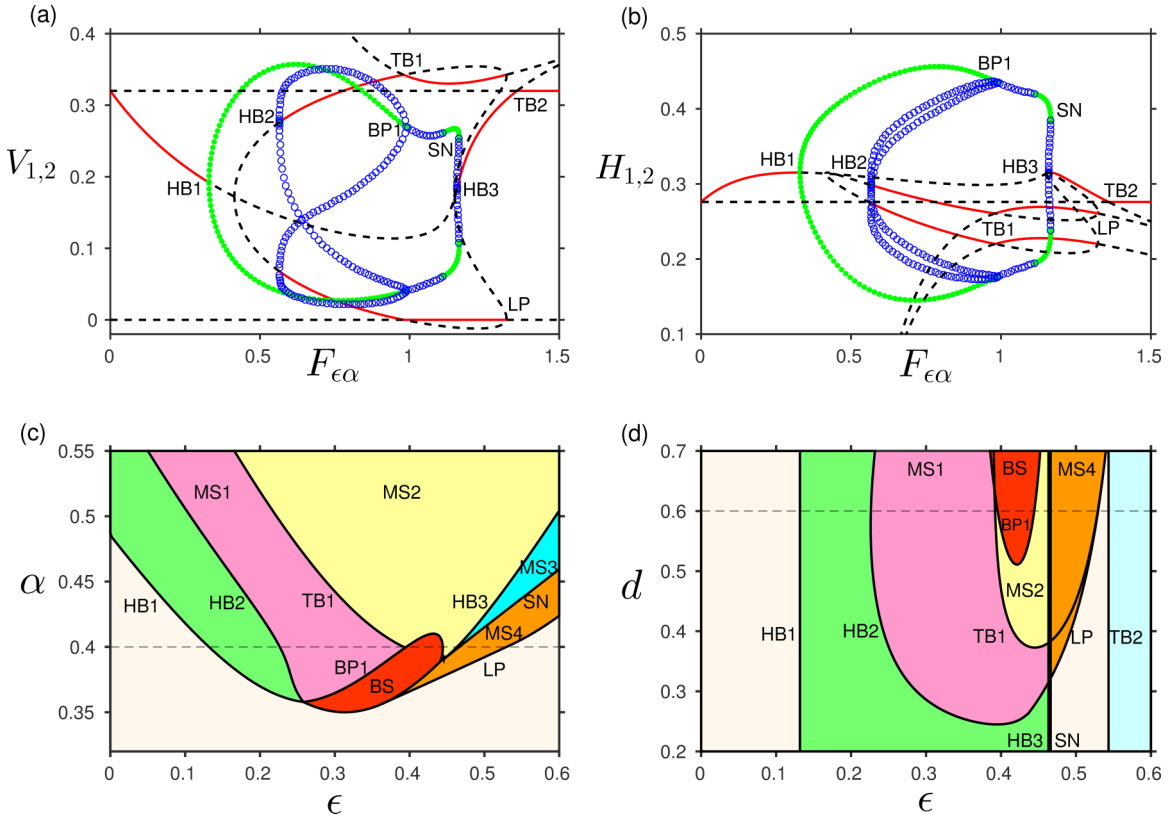

FIG. 2. One- and two-parameter bifurcation diagrams depicting multistability: (a) one-parameter bifurcation diagram of the resource (V_i) at different fraction $F_{\epsilon\alpha}$ with $\alpha = 0.4$ and $d = 0.6$, (b) one-parameter bifurcation diagram of the consumer (H_i) at different fraction $F_{\epsilon\alpha}$ with $\alpha = 0.4$ and $d = 0.6$, (c) ϵ-α space as a two-parameter bifurcation diagram, and (d) ϵ-d space as a two-parameter bifurcation diagram. The dotted lines denote a particular case representing (a) and (b). Here the consumption rates in both of the patches are identical ($\epsilon_1 = \epsilon_2 = \epsilon$). In (a) and (b), green and blue circles denote stable and unstable limit cycles, respectively, whereas solid red and dashed black curves denote stable and unstable steady states, respectively. Here HB, TB, BP, SN, and LP denote Hopf bifurcation, transcritical bifurcation, branch point, saddle-node, and limit point, respectively. BS and MS denote the region of bistability and multistability, respectively. Other parameters are $r = 0.55$, $K = 0.55$, $\alpha_i = 0.4$, $B = 0.16$, $\beta = 0.75$, $m = 0.2$, $\gamma = 0.6$, $r_1 = 0.5$, $K_1 = 0.6$, and $C = 0.6$.

species (V_i) and the consumer species (H_i) are shown in Figs. 2(a) and 2(b), respectively, at a particular dispersal rate ($d = 0.6$). Here the stable steady states and the stable limit cycles are represented by red solid curves and green filled circles, respectively. Further, the unstable steady states and the unstable limit cycles are denoted by black dashed curves and blue filled circles, respectively.

In Fig. 2(a), we observe that for both the lower and higher fractions $F_{\epsilon\alpha}$, simple dynamics with either stable steady states or oscillatory states occur. However, *multistability* consisting of *two stable steady states* and *one oscillatory state* is created through a subcritical Hopf bifurcation at HB2 ($F_{\epsilon\alpha} \approx 0.5655$). Subsequently, there exists another multistability through transcritical bifurcation at TB1 ($F_{\epsilon\alpha} \approx 0.98$) in which one of the steady states here reaches zero, i.e., the species becomes extinct in one of the states of multistability. Thereafter, multistability consisting of only stable steady states exists after the saddle-node bifurcation of the limit cycle (SN). Together with multistability, the coupled system also shows bistability for intermediate fractions, particularly between the bifurcation points BP1 and saddle-node bifurcation of the limit cycle (SN). The corresponding dynamics for the consumer populations (H_i) are shown in Fig. 2(b).

As the defined fraction $F_{\epsilon\alpha}$ measures the magnitude of consumer interactions on a local resource over a shared environmental resource, the complete dynamics for a wide range of local predation and environmental predation are also studied; the resulting two-parameter bifurcation diagram in ϵ-α space is shown in Fig. 2(c). One can easily observe that, at low predation in a local resource (α), the metacommunity experiences simple stable steady-state dynamics. However, various multistable regions (MS1, MS2, MS3, and MS4) and a bistable region (BS) arise [see Fig. 2(c)] for a wide range of parameter values. The time series in each multistable region shows different characteristics, later shown in Fig. 3. Since dispersal through simple diffusive coupling influences the dynamics of metacommunity, we further explore the dynamics of the coupled system for a wide range of dispersal rate d. We show multistable and bistable regions using the two-parameter bifurcation diagram in ϵ-d space [Fig. 2(d)]. Importantly, for the low and high values of the consumption rate (ϵ), the coupled system exhibits either a simple steady state or synchronized oscillations, whereas the intermediate consumption rate (ϵ) enables bistable and multistable dynamics in the coupled system. Indeed, Figs. 2(a) and 2(b) depict this observation in the exemplary bifurcation diagrams along the dotted horizontal lines of Figs. 2(c) and 2(d) (for $\alpha = 0.4$ and $d = 0.6$).

2. Basin stability measure

At different fractions ($F_{\epsilon\alpha}$), the coupled system (1) shows various characteristics of bistability and multistability. The time series in each multistable region, denoted as MS1, MS2, MS3, and MS4, are shown in the left panel of Fig. 3. For a fixed set of parameters, various initial conditions determine the alternative states arising in a multistable region. As far as time series are concerned, the coupled system shows three alternative steady states in MS1 [Fig. 3(a)] including one stable oscillatory state and two stable steady states, all of which have nonzero species density. But in MS2 [Fig. 3(b)], one of the steady states reaches zero density, i.e., the species becomes extinct. Similarly, three alternative stable steady states arise in MS4 [Fig. 3(c)], one of which is in the extinction state. In MS3 [Fig. 3(d)] there exist four alternative states, also denoting one stable oscillatory state and three stable steady states, one of which is in the extinction state. Indeed, one of the alternative states is zero in each of MS2, MS3, and MS4. Therefore, the considered coupled system with dispersal and a dynamic environment can experience a sudden transition from a species-rich state to a species-extinct state with variations in $F_{\epsilon\alpha}$.

Different initial conditions determine the respective converging state in a multistable region. Indeed, if the chosen initial condition is on a particular basin of attraction, then the system will reach the respective steady state. In contrast to choosing initial conditions from a particular basin of attraction, what is the probability of reaching the particular steady state in a multistable system if initial conditions are chosen randomly in the state space? This probability can be measured by the so called "basin stability." Henceforth, we use the concept of basin stability [25] to determine the characteristics of alternative steady states. Indeed, the probability (P_{S_i}) of reaching a particular state (S_i) in terms of percentage is computed as

$$P_{S_i} = \frac{\text{Number of simulations reaching a state } S_i}{\text{Total number of simulations}} \times 100.$$

Here, initial conditions are chosen randomly from the range $V_i \in [0,\ 0.45]$, $H_i \in [0,\ 0.5]$, and $E \in [0,\ 0.55]$. These ranges are taken from the one-parameter bifurcation diagrams of each variable [for V_i and H_i in Figs. 2(a) and 2(b), respectively]. By exploring each multistable region with 10^4 simulations in which initial conditions are chosen randomly and are uniformly distributed in the aforementioned ranges, we calculate the probability of reaching a particular state after removing enough transients from the time series.

For each alternative state in different multistable regions, the probability of reaching a particular state (P_{S_i}) is represented in the right panel of Fig. 3 using a pie chart with the same color coding as was used in the corresponding time series (also each state and the corresponding basin stability are marked with a number) in the left panel. As far as the basin stability is concerned, stable oscillations dominate in MS1 since oscillations arise for almost 85% of the considered initial conditions. In contrast, all three alternative states are equally distributed in MS2. Importantly, one of the states reaches zero (34%), hence the species has a better chance of survival in this case. Subsequently, the stable state (i.e., solid red curve) dominates (83%) in MS4 as compared to other alternative states. Finally, in MS3, the stable oscillatory state and all the remaining stable states are almost equally distributed. Importantly, in all these cases presented in Fig. 3, the system has less of a chance of reaching the lower-density state and/or the zero-density state. The basin stability of this low-density state is much lower in comparison with that of the other steady states.

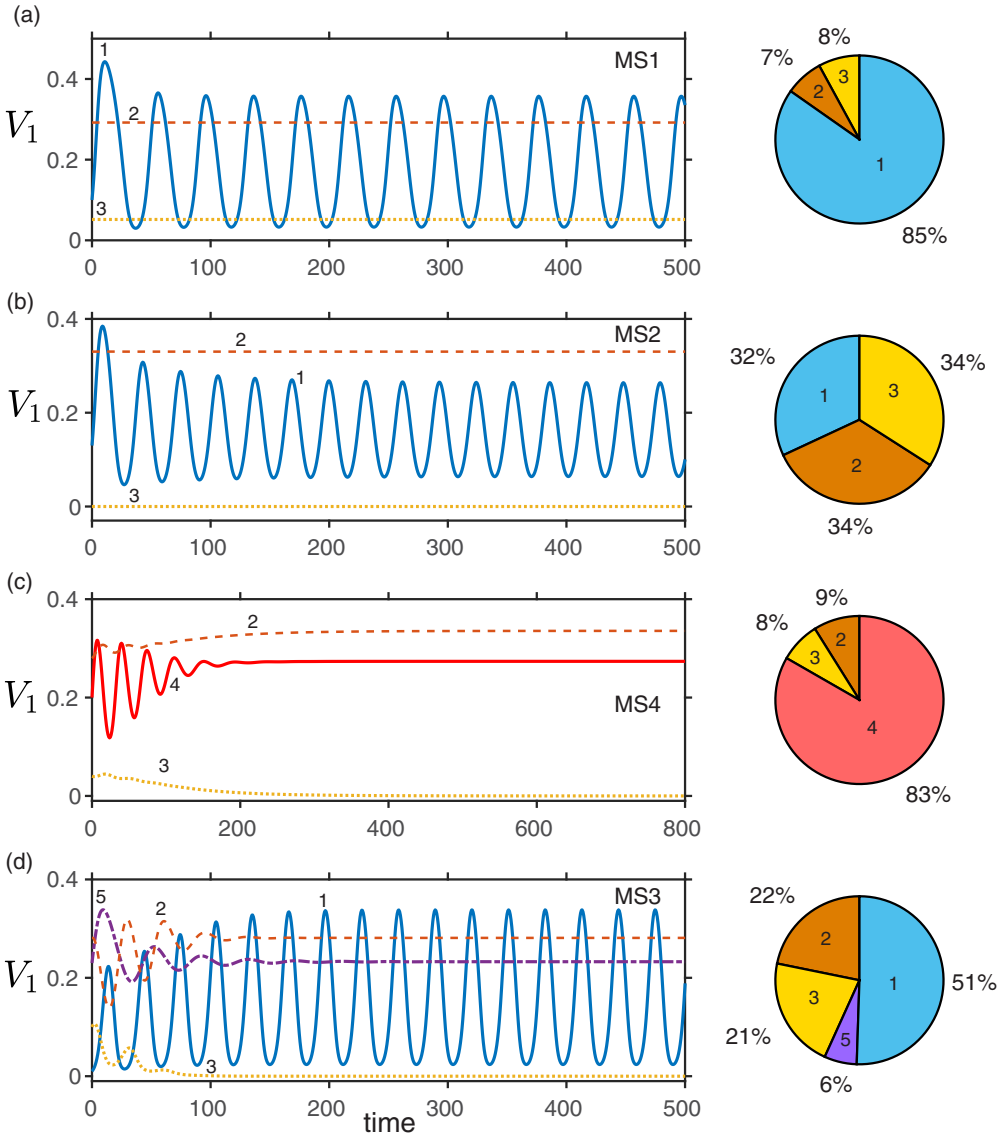

FIG. 3. Time series and the corresponding basin stability measures: In the left panel, each time series is set with an index, whereas the right panel denotes the percentage of corresponding dynamics from 10^4 simulations with random initial conditions. Multistability (a) MS1 for $\epsilon = 0.25$ and $\alpha = 0.4$, (b) MS2 for $\epsilon = 0.45$ and $\alpha = 0.4$, (c) MS4 for $\epsilon = 0.5$ and $\alpha = 0.4$, and (d) MS3 for $\epsilon = 0.55$ and $\alpha = 0.45$. The stable oscillations shown here are synchronized in both the interacting patches. Other parameters are $d = 0.6$, $r = 0.55$, $K = 0.55$, $B = 0.16$, $\beta = 0.75$, $m = 0.2$, $\gamma = 0.6$, $r_1 = 0.5$, $K_1 = 0.6$, and $C = 0.6$.

B. Effects of variations in the magnitude of consumer interactions over a shared resource ($F_{\epsilon_1\epsilon_2}$)

Instead of using the magnitude based on the local (V) and the shared (E) resources, now we define another form of magnitude only based on the dynamic environment. As mentioned earlier, the dynamic environment acts as a shared resource to the consumer species in all the interacting patches. As far as natural systems are concerned, the consumer's consumption rate over a shared resource in each patch can vary as well as having a different influence. In particular, a habitat structure and heterogeneity force the consumer species to have a heterogeneous effect on the dynamic environment. Emphasizing the distinct consumption rates ϵ_i of the shared resource E in each patch, here we define the magnitude (or fraction) as a ratio between the patch-1 consumption rate (ϵ_1) over the patch-2 consumption rate (ϵ_2):

$$F_{\epsilon_1\epsilon_2} = \frac{\epsilon_1}{\epsilon_2} = \frac{H_1 \text{ consumption rate over } E}{H_2 \text{ consumption rate over } E}.$$

As far as local dynamics are concerned, each patch has identical local interactions, but heterogeneity is set in the consumption rate (ϵ_i) over the environmental resource (E) only. Indeed, all patches have identical local dynamics without coupling and nonidentical dynamics over environmental coupling with E.

1. *Existence of multistability with variations in $F_{\epsilon_1\epsilon_2}$*

Now we explore the qualitative dynamics of the coupled system in terms of the defined magnitude of consumer interactions over the shared resource E. In particular, using one-parameter bifurcation diagrams for varying the fraction

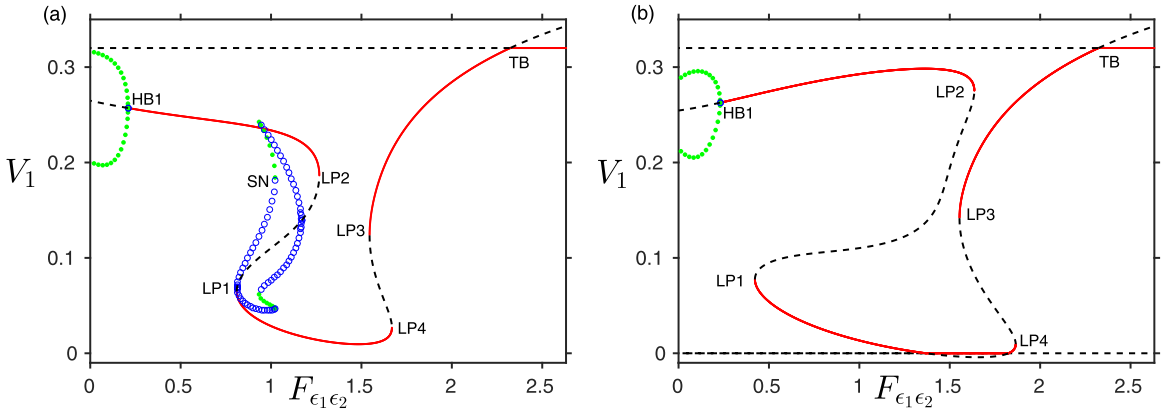

FIG. 4. (a) One-parameter bifurcation diagram for varying the fraction of consumption in the environmental resource ($F_{\epsilon_1\epsilon_2}$) for $d = 0.4$, and (b) one-parameter bifurcation diagram for varying the fraction of consumption in the environmental resource ($F_{\epsilon_1\epsilon_2}$) for $d = 0.8$. Other parameters are $r = 0.55$, $K = 0.5$, $\alpha_i = 0.4$, $B = 0.16$, $\beta = 0.75$, $m = 0.2$, $\gamma = 0.6$, $r_1 = 0.5$, $K_1 = 0.6$, and $C = 0.6$.

($F_{\epsilon_1\epsilon_2}$) at two different dispersal rates, the formation of multistability is shown in Fig. 4. Indeed, for increasing the fraction ($F_{\epsilon_1\epsilon_2}$) at the dispersal rate $d = 0.4$ in Fig. 4(a), the coupled system exhibits phase-synchronized oscillations that further lead to stable steady states at HB1. Between the limit points LP1 and LP2, and also between LP3 and LP4, two different hysteresis regions are formed with multistable and bistable behaviors. The multistable region consisting of phase-synchronized oscillations and two stable steady states exist through a saddle-node bifurcation of the limit cycle (SN). Subsequently, at the limit point (LP1), the resource density (V_1) reaches a low-density state that further leads to another hysteresis region between LP3 and LP4. Moreover, a higher fraction ($F_{\epsilon_1\epsilon_2}$) suppresses the resource density V through a transcritical bifurcation (TB). For another higher dispersal rate ($d = 0.8$), similar qualitative dynamics arises, which is shown in Fig. 4(b). In this case also, two hysteresis regions are formed that consist of three alternative stable steady states.

For a wide range of dispersal rate d and the fraction of consumer interactions $F_{\epsilon_1\epsilon_2}$, the complete dynamics are shown in Fig. 5 through a two-parameter bifurcation diagram in the $F_{\epsilon_1\epsilon_2}$-d plane. The bistable (BS1, BS2, and BS3) and multistable regions (MS1 and MS2) are shown in different shaded regions that are separated by bifurcation curves. Since the coupled system shows bistability and multistability as a combination of both equilibrium (Eq) and nonequilibrium (NEq) dynamics, we have represented these regions with the words Eq and NEq. In MS1, three different alternative

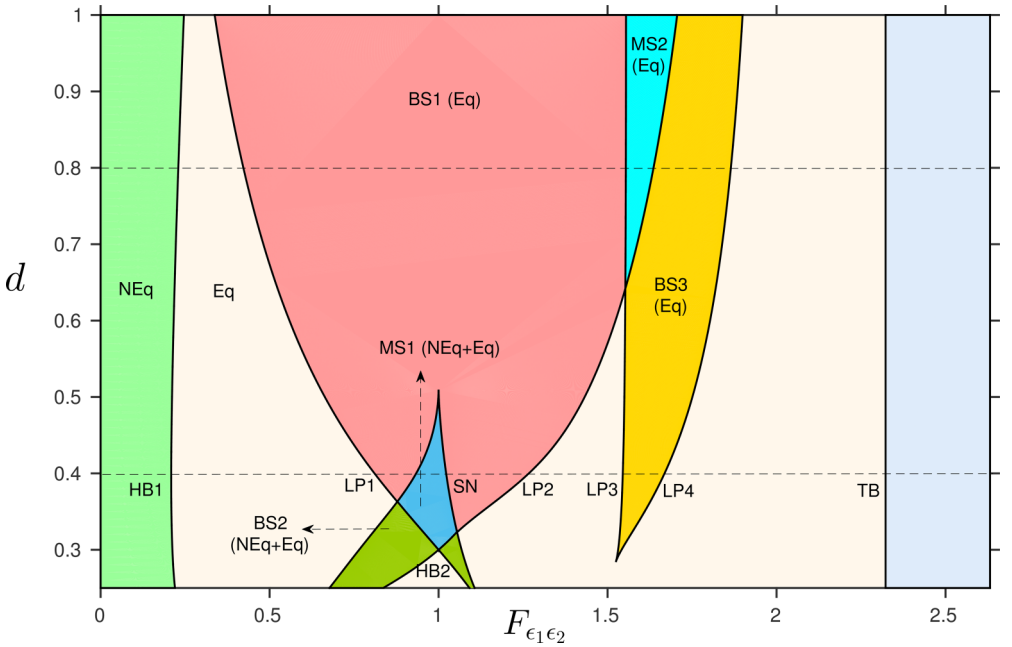

FIG. 5. Two-parameter bifurcation diagram with variations in $F_{\epsilon_1\epsilon_2}$ and d: Here Eq and NEq denote equilibrium (steady states) and nonequilibrium dynamics (oscillations), respectively. The bistable and multistable regions are denoted by BS and MS, respectively. Other parameters are $r = 0.55$, $K = 0.5$, $\alpha_i = 0.4$, $B = 0.16$, $\beta = 0.75$, $m = 0.2$, $\gamma = 0.6$, $r_1 = 0.5$, $K_1 = 0.6$, and $C = 0.6$.

states such as one nonequilibrium (NEq) and two equilibrium (Eq) states arise, whereas three alternative equilibrium states exist in MS2. Similarly, the bistability region (BS1) has two alternative equilibrium states, BS2 has one nonequilibrium and one equilibrium state, and finally BS3 has two alternative equilibrium states. The rightmost region in Fig. 5, denoted after the transcritical bifurcation (TB) line, represents the extinction of a shared environmental resource E. In Fig. 5, the dotted lines at the dispersal rates $d = 0.4$ and 0.8 correspond to the particular cases shown in Figs. 4(a) and 4(b), respectively. Similar to Fig. 3, here also one can determine the probability of reaching a particular state in bistable and multistable regions using the basin stability measure.

2. Critical transitions in the presence of random fluctuations

Biological populations are often influenced by random environmental fluctuations as a result of weather conditions, climate change, etc. Environmental stochasticity directly impacts community stability and persistence. In line with this reasoning, here we explore the coupled system in the presence of stochasticity. At first, we denote the coupled system (1) without stochasticity as

$$\frac{dX}{dt} = F(X), \tag{2}$$

where $X = [V_1\, H_1\, V_2\, H_2\, E]^T$, and $F(X)$ is the function representing consumer-resource interactions with both of the couplings. Stochasticity in ecological models has been used in different ways, such as intrinsic and extrinsic noise [29–32]. In [30], the dynamics of a generalized Lotka-Volterra competition model have been studied under the presence of additive and multiplicative noise, and it has been shown that multiplicative noise can induce coherent oscillations in the species. Here we consider stochasticity in the form of multiplicative *extrinsic* noise (also the behavior of the system under the influence of *intrinsic* stochastic fluctuation is shown in Appendix). After incorporating stochasticity in Eq. (2), the coupled system becomes

$$\frac{dX}{dt} = F(X) + \sigma X \xi(t), \tag{3}$$

where σ denotes the noise intensity and $\xi(t)$ denotes Gaussian white noise with zero mean and unit variance.

Similar to the deterministic case (i.e., Fig. 4), here we explore the stochastic system [Eq. (3)] using the defined magnitude ($F_{\epsilon_1\epsilon_2}$) of consumer interactions over the environmental resource. We numerically simulate the system using the Euler-Maruyama method [33] for varying the fraction $F_{\epsilon_1\epsilon_2}$ in two different ways. First, we simulate the system to increase the fraction from low to high, and second, we decrease the fraction from high to low. At the dispersal rate $d = 0.4$, the stochastic coupled system is explored to increase the fraction $F_{\epsilon_1\epsilon_2}$ from 0.5 to 2.1 within the time frame 2×10^3 in Fig. 6(a). The stochastic system follows its deterministic skeleton. At a particular threshold ($F_{\epsilon_1\epsilon_2} \approx 1.267$), after reaching very close to the SN bifurcation point, the system experiences a critical transition through suddenly changing its present state to another alternate state (low-density state) represented by arrow marks. A further increase in the fraction leads to another transition at $F_{\epsilon_1\epsilon_2} \approx 1.668$ from the lower to the upper state. The stochastic system experiences two transitions, upper to lower states and lower to upper states [Fig. 6(a)]. In contrast to an increase in fraction, if we decrease the fraction ($F_{\epsilon_1\epsilon_2}$) with the same range and also with the same noise intensity, two other transitions arise: upper to lower state at $F_{\epsilon_1\epsilon_2} \approx 1.47$ and further lower to upper state before $F_{\epsilon_1\epsilon_2} \approx 0.77$ [shown in Fig. 6(b)].

At the dispersal rate $d = 0.8$, Figs. 6(c) and 6(d) also show critical transitions for an increase and a decrease in the fraction $F_{\epsilon_1\epsilon_2}$, respectively. For example, for increasing the fraction in Fig. 6(c) with the same noise intensity $\sigma = 0.009$, there exists a transition at $F_{\epsilon_1\epsilon_2} \approx 1.636$. However, for decreasing the fraction in Fig. 6(d), two transitions occur from upper to lower at the threshold $F_{\epsilon_1\epsilon_2} \approx 1.49$ and further from lower to upper before the threshold $F_{\epsilon_1\epsilon_2} \approx 0.496$. Hence, the magnitude of consumer interactions in each patch on the resource E exhibits multiple critical transitions under the presence of stochasticity in the system.

3. Precursors of critical transitions

In the vicinity of a bifurcation point, the dominant eigenvalue reaches close to zero and the recovery rate from perturbations becomes increasingly slow, which is known as the critical slowing down [27]. In the case of a bifurcation-induced critical transition, critical slowing down indicators, which are generally known as early warning signals (EWS), such as lag-1 autocorrelation [AR(1)] and variance, are known to forewarn of an upcoming transition [34,35]. The cases of failed or misleading warnings of critical transitions are also reported in the literature [36,37]. Here, we explore the robustness of EWS in predicting critical transitions in the metacommunity system.

In our analysis, we consider stochastic time series of model (3) for both forward and backward transitions, as depicted in Figs. 6(a) and 6(b), respectively. In both time series, we first visually identify shifts between high to low resource density. Then we take time series segments [the boxed regions in Figs. 6(a) and 6(b)] prior to a critical transition and analyze them for the presence of EWS. For stationarity in residuals, we use the Gaussian detrending with a filtering bandwidth 60 before performing any statistical analysis of the data. Then we use a moving window size of half the length of the residual time series segment. The time series analyses have been performed using the Early Warning Signals Toolbox [38]. We calculate the lag-1 autocorrelation and the variance, as these two indicators are known to be most appropriate to anticipate critical transitions. The autocorrelation at lag-1 is given by $\rho_1 = \dfrac{E\{[x(t)-\mu][x(t+1)-\mu]\}}{\sigma^2}$, where E is the expected value operator, and $x(t)$ is the value of the state variable at time t. μ and σ^2 are the mean and the variance of $x(t)$, respectively. Variance is the second moment around the mean μ, and it is measured as $\sigma^2 = \frac{1}{N}\Sigma_{i=1}^{N}[x(t)-\mu]^2$, where N is the number of observations within the considered moving window. A concurrent rise in these indicators is known to forewarn of an upcoming regime shift [27,34,35].

In the case of anticipating forward transition, Fig. 7(a) depicts that neither the AR(1) nor the variance shows a

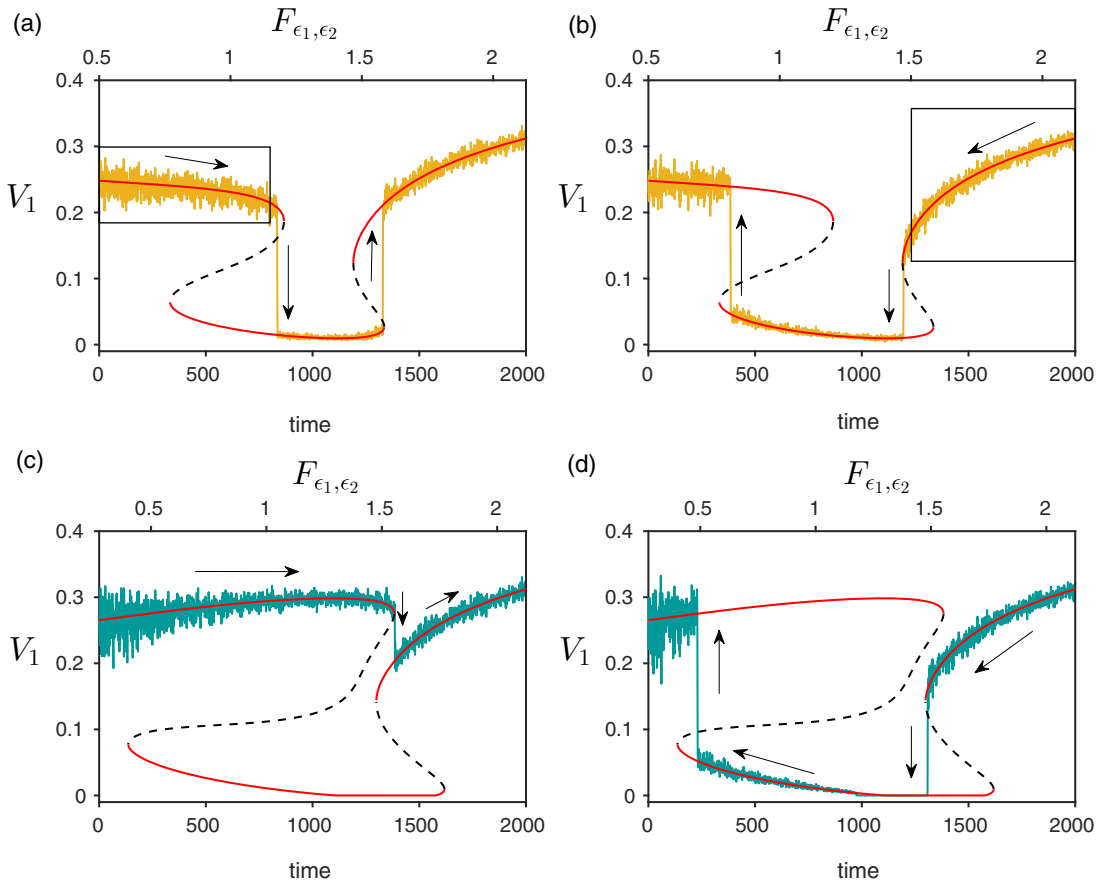

FIG. 6. Critical transitions using multiplicative noise for $d = 0.4$ when (a) $F_{\epsilon_1\epsilon_2}$ varies in the forward direction, and (b) $F_{\epsilon_1\epsilon_2}$ varies in the reverse direction. Critical transition for $d = 0.8$ when (c) $F_{\epsilon_1\epsilon_2}$ varies in the forward direction, and (d) $F_{\epsilon_1\epsilon_2}$ varies in the reverse direction. Other parameters are $\sigma = 0.009$, $r = 0.55$, $K = 0.5$, $\alpha_i = 0.4$, $B = 0.16$, $\beta = 0.75$, $m = 0.2$, $\gamma = 0.6$, $r_1 = 0.5$, $K_1 = 0.6$, and $C = 0.6$.

concurrent rise in their value, and hence they fail to predict an upcoming transition. However, for the backward transition, Fig. 7(b) depicts that both the AR(1) and the variance show a concurrent rise in their value. Hence, in this case AR(1) and the variance are able to successfully forewarn of a critical transition in species density. Though a critical transition is associated with the saddle-node bifurcation in both cases, we find that still in one case the EWS are unable to detect a transition beforehand. This predicts that CSD-based EWS are not always able to successfully detect a critical transition even if it is associated with a saddle-node bifurcation [37]. These results suggest that more investigations are still needed to understand EWS of critical transitions.

C. Multistability and multiclustering in a network structure

In natural ecosystems, typically a large number of habitats are connected through dispersal along with the shared dynamic environment. Here, we explore the coupled system (1) further for a network structure consisting of 16 patches under an environment-dependent framework. The considered network follows similar assumptions to those of Fig. 2, i.e., all patches are set to have identical dynamics in consumer-resource interactions. As in Fig. 2, here also we analyze the effects of variations in the magnitude of consumer interactions on local and shared resources.

We observe that here the network also shows multistability; additionally it shows multiclustered steady states. Figure 8 shows the spatiotemporal dynamics of the network for a particular set of fixed parameters. Depending upon initial conditions, here the system depicts either oscillatory or steady-state dynamics. In the oscillatory case, the interconnected patches show synchronized oscillations [Figs. 8(a) and 8(d)] that form a 1-cluster solution. Two different cases of alternative stable steady states are shown using spatiotemporal plots in Figs. 8(b) and 8(c). As far as stable steady states are concerned, multiclustering (n-cluster) arises in the network structure. For example, a 3-cluster and a 5-cluster are shown in Figs. 8(e) and 8(f), respectively.

As randomly chosen initial conditions are associated with the previously calculated basin stability, the network of 16 patches has high a probability of exhibiting equilibrium dynamics (stable steady states) rather than exhibiting nonequilibrium dynamics (synchronized oscillations). Due to the high dimensionality of the network, the probability of reaching the synchronized state is much lower (we find it to be less than 1%). Hence, the network structure with dispersal

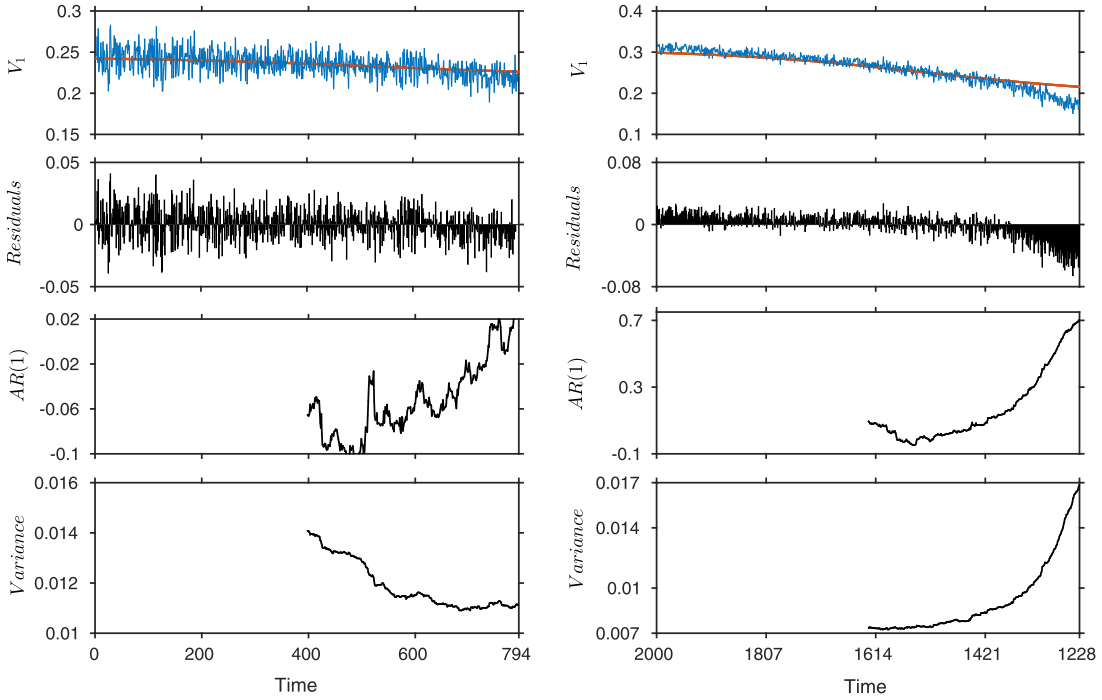

FIG. 7. Early warning signals calculated from the simulated time series data of the stochastic model [Eq. (3)] in the case of forward [see Fig. 6(a)] and backward [see Fig. 6(b)] transitions with variations in $F_{\epsilon_1\epsilon_2}$. The lag-1 autocorrelation [AR(1)] and the variance are calculated using a moving window of half the length of the time series segments [segments are indicated by the boxed regions in Figs. 6(a) and 6(b)]. (a) In the case of forward transition, neither AR(1) nor variance gives a reliable signal of an upcoming transition. (b) In the case of a backward transition, both indicators show a clear increasing trend and reliably indicate an upcoming critical transition. For more details, see the text.

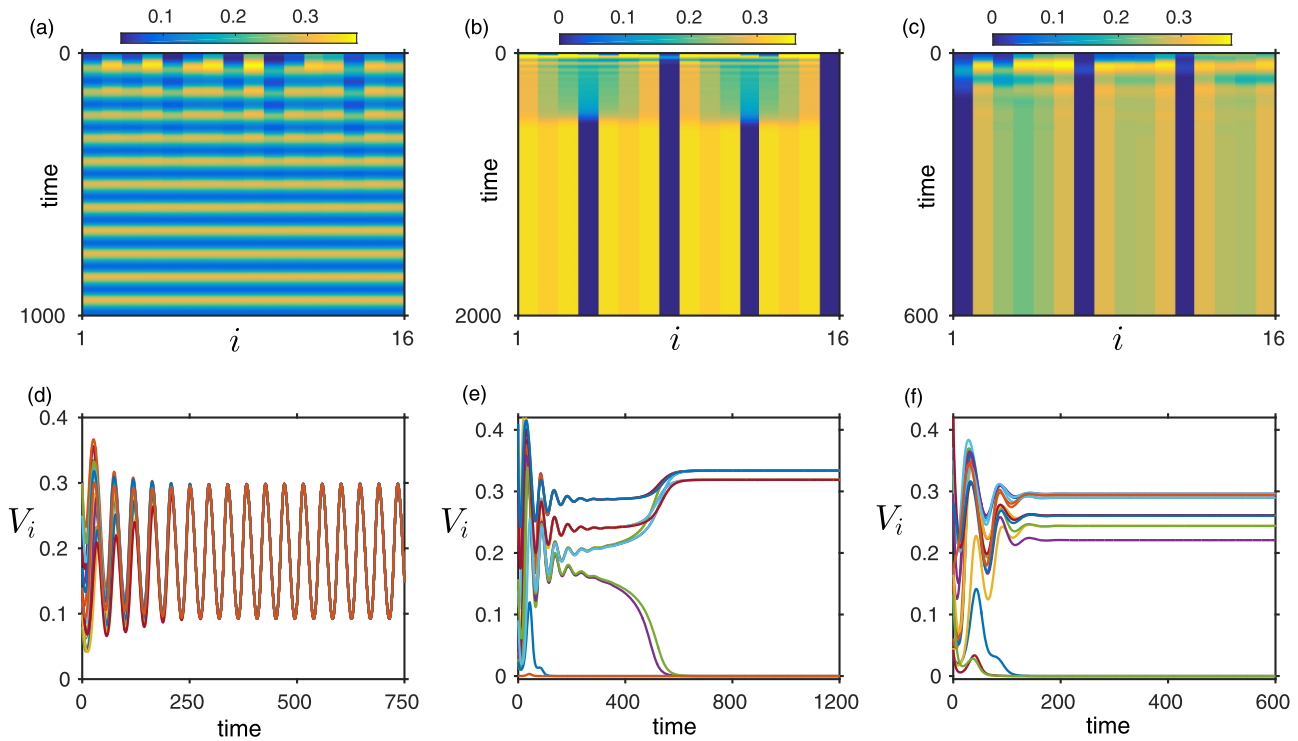

FIG. 8. Synchronization, multiclustering, and species extinction in a network of 16 patches: Spatial dynamics are represented in the top panel, and the respective temporal dynamics are represented in the bottom panel. (a),(d) Synchronized oscillations of 16 patches form 1-cluster; (b),(e) dynamics of stable steady states with three clusters in which one of the clusters reaches the critical zero state and species become extinct; and (c),(f) dynamics of stable steady states with multiple clusters that contain both nonzero and zero species density. The parameter values are $d = 0.5$, $\epsilon = 0.06$, $r = 0.55$, $K = 0.55$, $\alpha_i = 0.4$, $B = 0.16$, $\beta = 0.6$, $m = 0.15$, $\gamma = 0.7$, $r_1 = 0.5$, $K_1 = 1.6$, and $C = 0.8$.

through simple diffusive coupling as well as environmental coupling has a high probability of exhibiting multicluster solutions.

The existence of multicluster solutions indicates the promotion of community stability and persistence. A higher clustering number promotes metacommunity stability by reducing extinction risk, whereas a 1-cluster/2-cluster has a strong chance of extinction through other external forces such as seasonal change and climatic conditions. Indeed, the synchronized oscillations of metacommunity have a high risk of extinction since local extinction in one of the patches may lead to global extinction in all the interacting patches [39–41]. In contrast, in n-clustering stable steady states, local extinction does not lead to extinction of other patch populations. Therefore, n-clustering promotes metacommunity stability and its persistence. In addition to multistability and multiclustering, species extinction also arises in certain patches of the network. For example, in Fig. 8(e) the existing three-cluster state includes the critical zero steady state. Similarly, species extinction in some patches occurs in Fig. 8(f) as well.

IV. DISCUSSION

Here, we have studied a metacommunity model consisting of a diffusive coupling and a dynamic environmental coupling. In particular, incorporating a nonlinear dynamic environment with spatial heterogeneity and the magnitude of environment coupling acting on the metacommunity at a time, we have found a set of environmental conditions that can promote community stability and persistence. As most of the earlier studies on coupled oscillators have used coupling strength in determining the qualitative dynamics, our approach was based on two different magnitudes that quantify the effect of a dynamic environment at temporal and spatial scales.

The coupled nonlinear system determines bistability, multistability, as well as critical transitions in the presence of noise, as compared to its uncoupled version, which just exhibits simple characteristics of monostability. Both the simple diffusive and the environmental coupling drive the system's dynamics from simple to complex, i.e., from monostability to multistability. Indeed, the defined magnitude enables various types of multistability consisting of three or more alternative states. Moreover, the existing multistability contains either only alternative stable steady states or alternative states in a combination of both stable equilibrium and stable nonequilibrium dynamics. In particular, in the nonequilibrium case, perfectly synchronized as well as phase-synchronized oscillations arise, whereas homogeneous and heterogeneous steady states arise in the case of stable equilibrium. Our results based on these defined magnitudes emphasize the persistence of metacommunity through the characteristics of multistability.

By emphasizing the random initial conditions in natural systems, we have found the probability of attaining a particular alternative state in multistable regions using the basin stability measure. Subsequently, two types of critical transitions, one of which is from a high species density to a low species density, and the other from a low species density to a high species density, are identified in a stochastic metacommunity model under an environment-dependent framework. The CSD-based EWS are able to detect an upcoming transition in one case, and in another case they fail to provide any warning. This highlights the need for more rigorous study of the effectiveness of EWS while predicting a critical transition. Further, a large number of patches in a network structure shows similar qualitative dynamics of multistability and species extinction. Dispersal and the dynamic environment enable multistability and multiclustering in the network structure with identical patchwise interactions. The alternative stable states of multistability, consisting of both stable oscillations (nonequilibrium) as well as stable steady states (equilibrium), illustrate the significance of dispersal, a nonlinear dynamic environment, and its distributions at temporal and spatial scales on species persistence.

In earlier studies, multistability was observed in natural systems as well as laboratory experiments [42,43] in various fields, including physics [44], biology [45], ecology [46], genetics [47,48], neuroscience [49,50], and climate science [51,52]. Various types of nonlinear complex systems in terms of weakly dissipative systems, coupled and spatially extended systems, and delayed feedback systems generate multistability [42]. Here as a spatially extended coupled system of biological populations, our results emphasize multistability and critical transitions using the magnitude defined on considered environmental coupling at temporal and spatial scales. As far as real natural systems are concerned, a range of ecological systems including lakes [26], coral reefs [53], oceans, forests, and deserts [54,55] go through the alternative stable states [27]. One of the main reasons for shifting between the alternative states in these natural systems is the positive feedback that drives the system toward alternative states. In agreement with this, the dynamic environment in our model acts as a positive feedback on consumer populations, and its migration enhances alternative stable states. Hence our study provides important insights of environmental heterogeneity through the set of environmental conditions to promote metacommunity stability.

In summary, the magnitudes based on environmental coupling over local species interactions provide important insights into the set of environmental conditions that can promote metacommunity stability and persistence. Further studies are needed, focusing on the effects of various types of coupling (dispersal) strategies with higher tropical interactions and temperature-induced environment in a metacommunity. Moreover, the current rapid climate change due to anthropogenic factors has had a profound impact on community persistence. Therefore, it is quite important to address further challenges that arise in nonautonomous ecosystem models due to seasonal forcing and rapid climatic variations.

ACKNOWLEDGMENTS

R.A. and P.S.D. acknowledge the financial support from the SERB, Department of Science and Technology (DST), India (YSS/2014/000057). S.S. acknowledges the financial support from DST, India under the scheme DST-Inspire (Grant No. IF160459).

TABLE I. Different types of fundamental processes for the consumer-resource model (1), their propensity, and the corresponding jump of species. Ω is the volume in which the processes occur. The symbols +1 and −1 in the column showing the jump of species (ν_μ) represent birth and death of the respective species.

Sl. no.	Elementary events	Processes	Propensity functions (a_μ)	Jump of species (ν_μ)
1.	$V_i + D \rightleftharpoons V_i + V_i$	Logistic growth of consumer	$rV_i\left(1 - \frac{V_i}{K\Omega}\right)$	$V_i = V_i + 1$
2.	$E + D \rightleftharpoons E + E$	Logistic growth of environment	$r_1 E\left(1 - \frac{E}{K\Omega}\right)$	$E = E + 1$
3.	$V_i + H_i \to V_i H_i$ $V_i H_i \to V_i + V_i$	Holling type-II processes of resource	$\frac{\alpha_i V_i}{V_i + B*\Omega} H_i$	$V_i = V_i + 1$; $V_i = V_i - 1$
4.	$H_i + V_i \to H_i V_i$ $H_i V_i \to H_i + H_i$	Holling type-II processes of consumer	$\beta \frac{\alpha_i H_i V_i}{V_i + B\Omega}$	$H_i = H_i + 1$; $H_i = H_i - 1$
5.	$E + H_i \to E H_i$ $E H_i \to E + E$	Holling type-II consumption of environment	$\gamma \frac{\epsilon_i E}{E + C\Omega} H_i$	$E = E - 1$;
6.	$H_i \to D$	Natural mortality of consumer	mH_i	$H_i = H_i - 1$
7.	$H_i \rightleftharpoons H_j$	Diffusion of consumer between ith and jth patches	dH_i	$H_i = H_i + 1$; $H_i = H_i - 1$

APPENDIX: MONTE CARLO SIMULATION OF THE STOCHASTIC MODEL

There are two major approaches used to take into account *intrinsic* fluctuations in dynamical systems. The first one is the master equation approach, in which the stochastic dynamics are encoded analytically [56]. However, the complexity of a master equation associated with a dynamical system precludes us from solving this equation analytically in most cases. The other approach is the Monte Carlo simulation approach, which is an exact numerical solution of the master equation and provides stochastic time series [57]. In general, the Monte Carlo simulation provides individual realizations of the Markov process. It was developed by Gillespie and used widely for studying a wide range of dynamical systems, such as population dynamics [58], chemical reaction dynamics [59], systems biology [60,61], and many more.

The consumer-resource model (1) studied in this paper exhibits different types of fundamental processes. These processes are (i) logistic growth of V_i, (ii) logistic growth of E_i, (iii) Holling type-II functional response associated with resource consumption by H_i, (iv) Holling type-II functional response associated with the growth of consumer H_i, (v) Holling type-II functional response associated with environmental resource consumption by H_i, (vi) natural mortality of H_i, and (vii) diffusion of H_i between spatially separated patches. We list these fundamental processes along with their propensity function (a_μ) and the corresponding jump of species (ν_μ) symbolically in Table I, where $\mu = 1, 2, \ldots, 17$ are the associated processes for the model (1).

In Table I, the symbol D represents death and the symbol Ω represents the volume of the system. The species vector for this model is $X = [V_1, H_1, V_2, H_2, E]$. Using the elementary events stated in Table I along with their propensity function, one can perform the Monte Carlo simulation and update the species vector X. To perform our simulation, we use the same parameters as used in Fig. 6(a). We use the direct Gillespie algorithm that generates two uniform random numbers (r_1 and r_2) in the interval $(0, 1)$. The time (t) for the next process to occur is updated (i.e., $t + \tau$) stochastically by the following rule:

$$\tau = \frac{1}{a_0} \ln\left(\frac{1}{r_1}\right),$$

where $a_0 = \sum_{j=1}^{\mu} a_j$. The index μ of the occurring process is given by the smallest integer satisfying

$$\sum_{j=1}^{\mu-1} a_j < r_2 a_0 \leqslant \sum_{j=1}^{\mu} a_j.$$

The system states are updated, $X(t + \tau) = X(t) + \Delta X_{\nu_\mu}$, and then the simulation proceeds to the next occurring time. ΔX_{ν_μ} represents the change in the species vector in the stochastic time interval τ. The details of the algorithm can be found in [57].

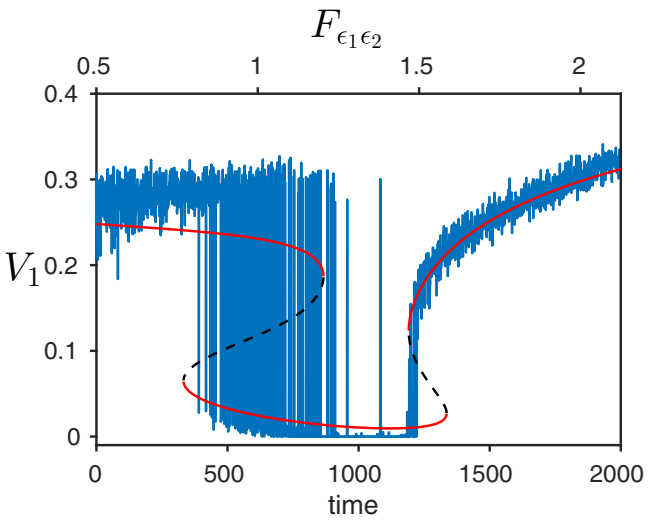

FIG. 9. The stochastic time series of the model (1), generated using the Gillespie algorithm, exhibits flickering between alternative states.

We find that the time series generated using the Monte Carlo simulation (that captures the intrinsic stochastic fluctuations) of the model exhibits flickering between alternative steady states (see Fig. 9). Due to flickering, the system switches back and forth between alternative states in response to relatively large stochastic fluctuations. Flickering between alternative steady states itself is known as an indicator of an impending critical transition [62]. Apart from that, variance as an EWS is known to work well for a flickering data set. Our result shows that if a metacommunity is affected by large stochastic perturbations, then it may exhibit flickering before completely shifting to an alternative state.

[1] A. Goldbeter, *Biochemical Oscillations and Cellular Rhythms: The Molecular Bases of Periodic and Chaotic Behaviour* (Cambridge University Press, Cambridge, 1996).

[2] A. Pikovsky, M. Rosenblum, and J. Kurths, *Synchronization: A Universal Concept in Nonlinear Sciences* (Cambridge University Press, Cambridge, UK, 2003).

[3] R. E. Mirollo and S. H. Strogatz, SIAM J. Appl. Math. **50**, 1645 (1990).

[4] M. G. Rosenblum, A. S. Pikovsky, and J. Kurths, Phys. Rev. Lett. **78**, 4193 (1997).

[5] S. H. Strogatz and I. Stewart, Sci. Am. **269**, 102 (1993).

[6] D. A. Vasseur and J. W. Fox, Nature (London) **460**, 1007 (2009).

[7] A. Koseska, E. Volkov, and J. Kurths, Phys. Rep. **531**, 173 (2013).

[8] Y. Kuramoto and D. Battogtokh, Nonlin. Phenom. Complex Syst. **4**, 380 (2002).

[9] A. M. Hagerstrom, T. E. Murphy, R. Roy, P. Hövel, I. Omelchenko, and E. Schöll, Nat. Phys. **8**, 658 (2012).

[10] T. Banerjee, P. S. Dutta, A. Zakharova, and E. Schöll, Phys. Rev. E **94**, 032206 (2016).

[11] T. Stankovski, T. Pereira, P. V. E. McClintock, and A. Stefanovska, Rev. Mod. Phys. **89**, 045001 (2017).

[12] V. M. Hunt and J. S. Brown, Theor. Ecol. **11**, 83 (2018).

[13] W. W. Murdoch, C. J. Briggs, and R. M. Nisbet, *Consumer-Resource Dynamics* (Princeton University Press, Princeton, NJ, 2003).

[14] J. E. Keymer, P. A. Marquet, J. X. Velasco-Hernandez, and S. A. Levin, Am. Nat. **156**, 478 (2000).

[15] G. L. Maser, F. Guichard, and K. S. McCann, J. Theor. Biol. **247**, 337 (2007).

[16] D. Gravel, E. Canard, F. Guichard, and N. Mouquet, PloS One **6**, 1 (2011).

[17] M. Holyoak, M. A. Leibold, and R. D. Holt, *Metacommunities: Spatial Dynamics and Ecological Communities* (University of Chicago Press, Chicago, 2005).

[18] R. Arumugam and P. S. Dutta, Phys. Rev. E **97**, 062217 (2018).

[19] S. Cenci, C. Song, and S. Saavedra, Ecol. Evol. **8**, 6852 (2018).

[20] B. Blasius, A. Huppert, and L. Stone, Nature (London) **399**, 354 (1999).

[21] M. Loreau, N. Mouquet, and R. D. Holt, Ecol. Lett. **6**, 673 (2003).

[22] E. Wall, F. Guichard, and A. R. Humphries, Theor. Ecol. **6**, 405 (2013).

[23] A. Gupta, T. Banerjee, and P. S. Dutta, Phys. Rev. E **96**, 042202 (2017).

[24] R. Arumugam, P. S. Dutta, and T. Banerjee, Phys. Rev. E **94**, 022206 (2016).

[25] P. J. Menck, J. Heitzig, N. Marwan, and J. Kurths, Nat. Phys. **9**, 89 (2013).

[26] M. Scheffer, S. Carpenter, J. A. Foley, C. Folke, and B. Walker, Nature (London) **413**, 591 (2001).

[27] M. Scheffer, *Critical Transitions in Nature and Society* (Princeton University Press, Princeton, NJ, 2009).

[28] B. Ermentrout, *Simulating, Analyzing, and Animating Dynamical Systems: A Guide to Xppaut for Researchers and Students (Software, Environments, Tools)* (SIAM, Philadelphia, 2002).

[29] L. J. Allen, *An Introduction to Stochastic Processes with Biology Applications* (Prentice Hall, Upper Saddle River, NJ, 2003).

[30] D. Valenti, A. Fiasconaro, and B. Spagnolo, Physica A **331**, 477 (2004).

[31] A. La Cognata, D. Valenti, A. A. Dubkov, and B. Spagnolo, Phys. Rev. E **82**, 011121 (2010).

[32] S. M. O'Regan and D. L. Burton, Bull. Math. Biol. **80**, 1630 (2018).

[33] D. J. Higham, SIAM Rev. **43**, 525 (2001).

[34] V. Dakos, S. R. Carpenter, W. A. Brock, A. M. Ellison, V. Guttal, A. R. Ives, S. Kéfi, V. Livina, D. A. Seekell, E. H. van Nes, and M. Scheffer, PLoS One **7**, e41010 (2012).

[35] M. Scheffer, S. R. Carpenter, T. M. Lenton, J. Bascompte, W. A. Brock, V. Dakos, J. van de Koppel, I. A. van de Leemput, S. A. Levin, E. H. van Nes, M. Pascual, and J. Vandermeer, Science **338**, 344 (2012).

[36] C. Boettiger and A. Hastings, Proc. R. Soc. London, Ser. B **279**, 4734 (2012).

[37] P. S. Dutta, Y. Sharma, and K. C. Abbott, Oikos **127**, 1251 (2018).

[38] http://www.early-warning-signals.org/.

[39] I. Hanski, Nature (London) **396**, 41 (1998).

[40] I. Hanski, Oikos **87**, 209 (1999).

[41] W. Gu, R. Heikkilä, and I. Hanski, Landscape Ecol. **17**, 699 (2002).

[42] U. Feudel, Int. J. Bifurcation Chaos **18**, 1607 (2008).

[43] A. N. Pisarchik and U. Feudel, Phys. Rep. **540**, 167 (2014).

[44] F. T. Arecchi, R. Meucci, G. Puccioni, and J. Tredicce, Phys. Rev. Lett. **49**, 1217 (1982).

[45] D. Angeli, J. E. Ferrell, and E. D. Sontag, Proc. Natl. Acad. Sci. (USA) **101**, 1822 (2004).

[46] R. M. May, Nature (London) **269**, 471 (1977).

[47] P. Smolen, D. A. Baxter, and J. H. Byrne, Am. J. Physiol.-Cell Physiol. **274**, C531 (1998).

[48] E. Ullner, A. Zaikin, E. I. Volkov, and J. García-Ojalvo, Phys. Rev. Lett. **99**, 148103 (2007).

[49] J. L. Schwartz, N. Grimault, J. M. Hupé, B. C. J. Moore, and D. Pressnitzer, Philos. Trans. R. Soc. London, Ser. B **367**, 896 (2012).

[50] J. A. S. Kelso, Philos. Trans. R. Soc. London, Ser. B **367**, 906 (2012).

[51] A. Robinson, R. Calov, and A. Ganopolski, Nat. Climate Change **2**, 429 (2012).

[52] V. Lucarini and T. Bódai, Nonlinearity **30**, R32 (2017).

[53] N. Knowlton, Am. Zool. **32**, 674 (1992).

[54] V. Brovkin, M. Claussen, V. Petoukhov, and A. Ganopolski, J. Geophys. Res.: Atm. **103**, 31613 (1998).

[55] M. Hirota, M. Holmgren, E. H. Van Nes, and M. Scheffer, Science **334**, 232 (2011).

[56] N. G. Van Kampen, *Stochastic Processes in Physics and Chemistry* (Elsevier, Amsterdam, 1992), Vol. 1.

[57] D. T. Gillespie, J. Comput. Phys. **22**, 403 (1976).

[58] A. J. Black and A. J. McKane, Trends Ecol. Evol. **27**, 337 (2012).

[59] D. T. Gillespie, Annu. Rev. Phys. Chem. **58**, 35 (2007).

[60] J. Paulsson, O. G. Berg, and M. Ehrenberg, Proc. Natl. Acad. Sci. (USA) **97**, 7148 (2000).

[61] J. W. Locasale, A. S. Shaw, and A. K. Chakraborty, Proc. Natl. Acad. Sci. (USA) **104**, 13307 (2007).

[62] R. Wang, J. A. Dearing, P. G. Langdon, E. Zhang, X. Yang, V. Dakos, and M. Scheffer, Nature (London) **492**, 419 (2012).